

# IRANIAN JOURNAL OF CHEMICAL ENGINEERING

## Chairman

Navid Mostoufi Professor, University of Tehran, Iran

## Editor-in-Chief

Masoud Rahimi Professor, Razi University, Iran

## Executive Director

Leila Sadafi-Nejad (M.Sc.)

## EDITORIAL BOARD

- ❖ Abbasian, J. (Associate Professor, Illinois Institute of Technology, USA)
- ❖ Badakhshan, A. (Emeritus Professor, University of Calgary, Canada)
- ❖ Barikani, M. (Professor, Iran Polymer and Petrochemical Institute, Iran)
- ❖ Jafari Nasr, M. R. (Professor, Research Institute of Petroleum Industry (RIPI), Iran)
- ❖ Karimi, I. A. (Professor, National University of Singapore, Singapore)
- ❖ Madaeni, S. S. (Professor, Razi University, Iran)
- ❖ Mansoori, G. A. (Professor, University of Illinois at Chicago, USA)
- ❖ Moghaddas, J. S. (Professor, Sahand University of Technology, Iran)
- ❖ Moosavian, M. A. (Professor, University of Tehran, Iran)
- ❖ Moshfeghian, M. (Professor, Shiraz University, Iran)
- ❖ Movagharnjad, K. (Professor, Babol University of Technology, Iran)
- ❖ Naseri, S. (Professor, Tehran University of Medical Sciences, Iran)
- ❖ Omidkhah, M. R. (Professor, Tarbiat Modares University, Iran)
- ❖ Pahlavanzadeh, H. (Professor, Tarbiat Modares University, Iran)
- ❖ Panjeshahi, M. H. (Professor, University of Tehran, Iran)
- ❖ Pazouki, M. (Professor, Materials and Energy Research Center (MERC), Iran)
- ❖ Rahimi, M. (Professor, Razi University, Iran)
- ❖ Rahimi, R. (Professor, University of Sistan and Baluchestan, Iran)
- ❖ Rashidi, F. (Professor, Amirkabir University of Technology, Iran)
- ❖ Rashtchian, D. (Professor, Sharif University of Technology, Iran)
- ❖ Shariaty-Niassar, M. (Professor, University of Tehran, Iran)
- ❖ Shayegan, J. (Professor, Sharif University of Technology, Iran)
- ❖ Shojaosadati, S. A. (Professor, Tarbiat Modares University, Iran)
- ❖ Soltanmohammadzadeh, J. S. (Associate Professor, University of Saskatchewan, Canada)
- ❖ Taghikhani, V. (Professor, Sharif University of Technology, Iran)
- ❖ Towfighi, J. (Professor, Tarbiat Modares University, Iran)

## INTERNATIONAL ADVISORY BOARD

- ❖ Arastoopour, H. (Professor, Illinois Institute of Technology, USA)
- ❖ Ataai, M. M. (Professor, University of Pittsburgh, USA)
- ❖ Barghi, Sh. (Assistant Professor, University of Western Ontario, Canada)
- ❖ Chaouki, J. (Professor, University of Polytechnique Montréal, Canada)
- ❖ Ein-Mozaffari, F. (Associate Professor, Ryerson University, Canada)
- ❖ Farnood, R. R. (Professor, University of Toronto, Canada)
- ❖ Jabbari, E. (Associate Professor, University of South Carolina, USA)
- ❖ Jand, N. (Assistant Professor, Università de L'Aquila, Italy)
- ❖ Lohi, A. (Professor, Ryerson University, Canada)
- ❖ Moghtaderi, B. (Professor, University of Newcastle, Australia)
- ❖ Mohseni, M. (Associate Professor, University of British Columbia, Canada)
- ❖ Nassehi, V. (Professor, Loughborough University, UK)
- ❖ Noureddini, H. (Associate Professor, University of Nebraska, USA)
- ❖ Rohani, S. (Professor, University of Western Ontario, Canada)
- ❖ Shahinpoor, M. (Professor, University of Maine, USA)
- ❖ Soroush, M. (Professor, Drexel University, USA)
- ❖ Taghipour, F. (Associate Professor, University of British Columbia, Canada)

\* This journal is indexed in the Scientific Information Database (<http://en.journals.sid.ir/JournalList.aspx?ID=3998>).

\* This journal is indexed in the Iranian Magazines Database ([www.magiran.com/maginfo.asp?mgID=4585](http://www.magiran.com/maginfo.asp?mgID=4585)).

\* This journal is indexed in the Islamic World Science Citation Center (<http://ecc.isc.gov.ir/showJournal/3561>).

Language Editor: Sajjad Saberi

Art & Design: Fatemeh Hajizadeh

Iranian Association of Chemical Engineers, Unit 11, No. 13 (Block 3), Maad Building, Shahid Akbari Boulevard, Azadi Ave., Tehran - Iran.

Tel: +98 21 6604 2719 Fax: +98 21 6602 2196

# Iranian Journal of Chemical Engineering

Vol. 16, No. 3 (Summer 2019), IChE

- Experimental and Computational Study on Hydrodynamic of a Downscaled Mini Vessel USP Dissolution Test Apparatus II** 3-22  
A. Mohammadi, J. S. Moghaddas
- Reactor Modeling and Kinetic Parameters Estimation for Diethyl Benzene (DEB) Dehydrogenation Reactions** 23-36  
M. E. Zeynali, H. Abedini, H. R. Sadri
- Nelder-Mead Algorithm Optimization and Galerkin's Method for Thermal Performance Analysis of Circular Porous Fins with Various Profiles in Fully Wet Conditions** 37-57  
M. R. Talaghat, F. Shafiei
- Effect of MgAl<sub>2</sub>O<sub>4</sub> Catalyst Support Synthesis Method on the Catalytic Activity of Nickel Nano Catalyst in Reverse Water Gas Shift Reaction** 58-69  
A. Ranjbar, S. F. Aghamiri, A. Irankhah
- Computational Fluid Dynamics Study of and GA Modeling Approach to the Bend Angle Effect on Thermal-Hydraulic Characteristics in Zigzag Channels** 70-83  
S. Salimi, R. Beigzadeh
- Two-Phase Flow Pressure Drop Calculation Using Homogeneous Equilibrium Model** 84-92  
M. Asadollahi
- Notes for Authors** 93

## Experimental and Computational Study on Hydrodynamic of a Downscaled Mini Vessel USP Dissolution Test Apparatus II

A. Mohammadi, J. S. Moghaddas\*

Transport Phenomena Research Center, Faculty of Chemical Engineering, Sahand University of Technology, P. O. Box: 51335/1996, Tabriz, Iran

---

### ARTICLE INFO

#### Article history:

Received: 2019-03-08

Accepted: 2019-09-29

---

#### Keywords:

Computational Fluid Dynamics (CFD), Hydrodynamics, Particle Image Velocimetry, Downscaled USP 2 Dissolution Apparatus

---

### ABSTRACT

Although not listed on the United States Pharmacopeia (USP), like standard USP 2, the small-volume USP 2 dissolution apparatus has gained a great deal of attention, especially for cases where a small number of drug products are available for testing in the research and design step or evaluations are to be conducted on a tablet containing trace amounts of active pharmaceutical ingredients. In this study, firstly, a small-volume USP 2 apparatus was designed and manufactured using downscaling rules with the standard USP 2 as a reference. Then, the velocity profile, flow patterns, and shear rate were obtained by PIV and COMSOL simulation software at paddle speeds of 66 and 133 rpm, corresponding to the agitation speeds of 50 and 100 rpm, respectively, in the standard USP 2. The comparison of the experimental and computational results showed acceptable agreement between the two. The instantaneous velocity data showed eddies and secondary flows in different zones of the vessel that are desirable for micro-mixing and, yet, undesirable in terms of system consistency and reproducibility, because samplings from these zones are known to generate inconsistent data. Furthermore, the increased agitation rate led to the disappearance of rotational zones around the paddle. The magnitude of velocity and shear rate increased by 35 % with an increment in paddle stirring from 66 to 133 rpm.

---

### 1. Introduction

In pharmaceutical industries, following the development of solid dosage forms such as tablets and capsules, it is necessary to carry out dissolution and release tests on the formulated samples to verify formulation of the dosage forms [1,2], adjust quality control standards [3], predict in vivo drug release and performance [3,4], and verify in vivo-in vitro correlation of the release date. United States Pharmacopeia (USP) has introduced four types of dissolution test apparatus along with

dissolution and disintegration standards to reproduce mechanical tensions that are exhibited by the gastrointestinal tract [5,6]. The most common apparatus used for dissolution and release testing is 1000-ml USP 2, wherein a rotating paddle is used to produce flow. This USP paddle apparatus has been widely used in pharmaceutical industries for about 40 years recently [5,7]. However, this apparatus alone cannot be effectively used for dissolution tests under particular conditions. For example, for effective

---

\*Corresponding author: jafar.moghaddas@sut.ac.ir

therapy, the dosage of particular APIs in solid dosage forms should be low so that toxicity in the body could be prevented. Therefore, during dissolution and release tests in a conventional USP 2, the concentration of the drug in the dissolution medium may decrease to a point so low beyond the limit of detection by conventional analysis methods, making the dissolution test data unreliable. In addition, most of the solid dosage forms have a prolonged release due to the presence of a poorly water-soluble drug substance [8], polymers with specific properties in the matrix structure [9], and hydrophobicity of the matrix [10]. Therefore, within a specified time span, only a small amount of API is likely to be released from the matrix structure and, thus, drug analysis by conventional analytical methods runs into difficulty. Recently, the small-volume USP 2 dissolution apparatus with a small paddle has gained much popularity due to its low material requirement, research efficiency due to the development of bio-relevant methods, and dosage forms related to pediatric populations [6]. Klein et al. (2006) obtained the release profiles of four types of drug substances in a 500-ml USP 2 dissolution apparatus. The results showed that the small-volume dissolution test apparatus could serve as a useful tool for determining the release profile of drug substances [11]. Emmanuel et al. (2010) studied the dissolution performance of different drug products with different release mechanisms in a 150-ml USP 2 dissolution apparatus [12]. Stamatopoulos et al. (2016) applied the PLIF technique to investigate hydrodynamics and release rate of rhodamine from tablets produced via the compression process in a 100-ml USP 2 apparatus at different viscosities [13]. Aoki et al. (1994) obtained the release profiles of two types of

drug tablet in a 250-ml USP 2 and compared the results with those of in-vivo tests [14]. In spite of the widespread application of small-volume USP 2, its features and design procedure are yet to be well documented. In order to standardize the apparatus to extend its application range, its design, downscaling, performance evaluation, and validation procedures must be investigated [1,7]. Studies showed that minor modifications to the apparatus geometry (e.g., slightly deviating from the paddle eccentrically, changing the clearance between the bottom of the paddle and that of the vessel, changing the radius of hemispherical bottom of the vessel, and changing the agitation rate) can affect the apparatus hydrodynamics and, consequently, the vivo-in vitro correlations [2,4]. Existing studies have investigated the effects of changes in the vessel size, shape, and agitation rate based on fluids mechanics, without considering the existing standard and downscaling rules. According to the existing standards [15], the agitation rate of conventional USP 2 paddle ranges from 25 to 75 rpm. However, some applications require the agitation rates of 50 to 100 rpm, and rarely 25 to 150 rpm. Bocanegra et al. (1990) studied the hydrodynamics of USP 2 apparatus using the LDA technique at a paddle agitation rate of 60 rpm [16]. Kukura et al. (2004) predicted the shear rate of the apparatus by studying the hydrodynamics of fluid flow at a paddle agitation rate of 100 rpm [2]. Stamatopoulos et al. (2015) examined the velocity field and the mixing pattern in a 100-ml USP 2 apparatus operating at an agitation rate of 50 rpm with fluids of different viscosities [6]. Baxter et al. (2005) used such engineering tools as PIV, PLIF, and CFD to study the fluid flow in a USP 2 at the paddle agitation rates of 50 and

100 rpm. Their findings included the velocity field, mixing pattern, shear rate, and moving pattern of a tablet during dissolution tests [17]. Bai et al. (2007) determined the magnitude and direction of velocity, shear rate, and turbulence kinetic energy in a 1000-ml USP 2 operating at a paddle rate of 50 rpm using LDV and CFD techniques [18]. In the present study, a 500-ml small-volume SUP 2 was designed and manufactured using downscaling rules and considering the specifications of a 1000-ml standard USP 2 as a reference. The commonly used agitation speed of the paddle in the 1000-ml standard USP 2 ranges from 50 to 100 rpm [19]. According to FIP guidelines, the corresponding agitation rates to the hydrodynamics of a 500-ml USP 2 apparatus were found to be 66 and 133 rpm. Therefore, the main purpose of this study is to investigate the hydrodynamics of the down-scaled small-volume USP 2 dissolution apparatus by determining fluid flow characteristics, velocity profile, and shear rate using engineering tools, namely PIV and COMSOL MULTIPHYSICS 5.2.

## 2. Experimental setup and methods

### 2.1. Small-volume USP 2 dissolution test apparatus

The small volume dissolution apparatus, with a capacity of 500 ml, used in this work is a downscaled model of a 1000-ml standard USP 2 dissolution apparatus composed of a round-bottom cylindrical vessel made of tempered Pyrex. Figure 1 and Table 1 present the dimension of the apparatus, based on which its volume could be calculated through the following relationship:

$$V = \frac{\pi D^2 H}{4} + \frac{\pi D^3}{12} \quad (1)$$

$$\text{Aspect ratio} = \frac{H}{D} = 1.6 \quad (2)$$

Accordingly by substituting Eq. (2) into Eq. (1) and assuming that  $D_s = 100$  mm (Table 2), the empty volume of the standard USP 2 apparatus used in this research was measured as  $V_s = 1518.2$  cm<sup>3</sup>. On the assumption that  $V_m = 0.422 V_s$ , the empty volume of a 500-ml USP 2 apparatus was calculated as  $V_m = 640$  cm<sup>3</sup>. Therefore, according to Eq. (1), the diameter of the downscaled vessel was obtained as  $D_m = 75$ mm. By taking the FIP guidelines into account, the agitation rate should be obtained in the 1000-ml USP 2 apparatus by stirring at 50 rpm [19]. According to the downscaling rules, the agitation rate corresponds to the hydrodynamics of the standard USP 2. The paddle diameter for a 500-ml USP 2 was calculated as follows:

i. For geometrically similar systems and identical liquid properties [20], the following equation is used:

$$N_s D_s = N_m D_m \quad (3)$$

According to Eq. (3), the agitation rate corresponding to the hydrodynamics of the standard USP 2 was found to be  $N_m = 66$  rpm.

ii. In order to maintain dynamic similarity, Froude (Fr) and Reynolds numbers (Re) must be simultaneously constant, which is simply impossible with scaling. Constant Fr is often used in the case of surface aeration in wastewater, where a stirrer is used on the air-water surface to aerate the liquid [20]. Constant Re can be considered in the case of a fully immersed stirrer. Therefore, we get:

$$Re_s = Re_m \quad (4)$$

$$N_s D_{p_s}^2 = N_m D_{p_m}^2$$

By computing Eq. (4) by known values, the paddle diameter of the 500-ml USP 2 was calculated as  $D_{p_m} = 64$  mm. The standard dimension ratio was used to determine the paddle's lower diameter and height.

$$\left(\frac{D_{p_u}}{D_{p_l}}\right)_s = \left(\frac{D_{p_u}}{D_{p_l}}\right)_m = \frac{74}{42} = 1.762 \quad (5)$$

On the assumption that  $(D_{p_u})_m = 64$  mm, the paddle's lower diameter in the 500-ml USP 2 was calculated, using Eq. (5), as  $(D_{p_l})_m = 36.3$  mm.

$$\left(\frac{D_p}{H_p}\right)_s = \left(\frac{D_p}{H_p}\right)_m = \frac{74}{19} = 3.895 \quad (6)$$

The height of the paddle of the 500-ml USP 2 apparatus was calculated as  $H_{p_m} = 16.4$  mm by assuming that  $D_{p_m} = 64$  mm in Eq. (6). The clearance rate between the bottom of the paddle and that of the vessel was calculated by a single-scale ratio,  $S$ , between the large (standard USP 2) and small-scale apparatus (model USP 2). By considering  $C_s = 25$  mm, the clearance for the 500-ml USP 2 was measured as  $C_m = 18.75$  mm.

$$S = \frac{D_m}{D_s} = \frac{C_m}{C_s} = \frac{75}{100} \quad (7)$$

According to FIP guidelines, the agitation rate should typically be obtained in the 1000-ml USP 2 apparatus by stirring at 100 rpm [19]. The agitation rate corresponding to the hydrodynamics of the standard USP 2 and dimensions of the 500-ml USP 2 was

calculated in the same way. The specifications of the downscaled USP 2 are given in Table 1. During the PIV experiments, the USP 2 vessel was placed in a square acrylic tank filled with water in order to keep its temperature constant while ruling out the effects of refractive index caused by the vessel curvature. Reynolds number and paddle tip speed corresponding to 66 and 133 rpm were 2749,  $0.221 \text{ m s}^{-1}$  and 5541,  $0.445 \text{ m s}^{-1}$ , respectively.

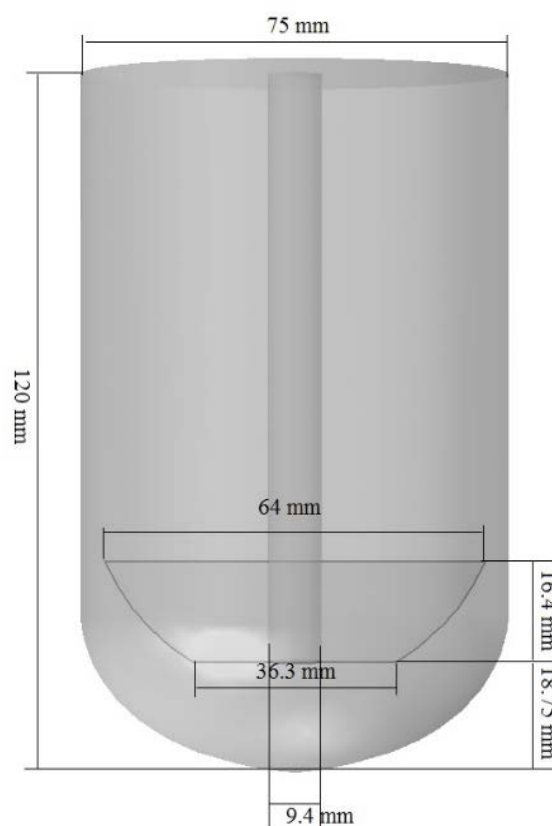


**Figure 1.** The dimension of small-volume USP 2 used in this work.

**Table 1**

Component Specification of 500 ml USP 2 dissolution test apparatus.

Component specification (mm)	Agitation speed of paddle (rpm)	$H_m$	$D_m$	The diameter of the shaft	Thickness of the paddle	$(D_{p_u})_n$	$(D_{p_l})_m$	$H_{p_m}$	$C_m$
	66	120	75	9.4	4.0	64	36.3	16.4	18.75
	133	120	75	9.4	4.0	64	36.3	16.4	18.75

**Table 2**

Component Specifications of 1000-ml USP 2 dissolution test apparatus according to Dissolution <711> Standard.

Internationally harmonized specification (mm)	$H_s$	$D_s$	Diameter of the shaft	Thickness of the paddle	$D_{pu}$	$D_{pl}$	$H_p$	$C_s$
	160	100	9.4-10.1	4.0	74.0-75.0	$42 \pm 1.0$	$19.0 \pm 0.5$	$25 \pm 2$

## 2.2. Study of PIV

Particle image velocimetry is a quantitative nonintrusive technique applicable to numerous mixing equipment items to determine flow patterns and velocity fields [21]. PIV system is composed of an Nd:YAG laser as its light source, CCD camera, synchronizer, and a computer for acquiring and processing the data and obtaining the hydrodynamic information of the tested USP 2. The light source emits two successive pulses of green laser light with a wavelength of 532 nm. Used to measure the velocity field, CCD camera is installed perpendicular to the emitted laser plane. Prior to the PIV experiments, the liquid inside the vessel is seeded by glass beads with a consistent

particle seeding density of  $1.01 \text{ g cm}^3$  [22] and a diameter of  $10 \mu\text{m}$ . The glass beads added to the liquid follow the fluid flow path and characterize the velocity field without any effect on flow specification. Davis software was utilized to acquire two successive digital images from the camera and analyze the raw data to obtain hydrodynamics information. For this purpose, 300 images were taken from the laser sheet by the CCD camera at each agitation rate of the paddle. PIV experiments were carried out at two agitation rates of 66 and 133 rpm corresponding to the typical agitation speeds of the standard USP 2 (50 and 100 rpm, respectively). Fig. 2 shows a schematic of the PIV experimental system.

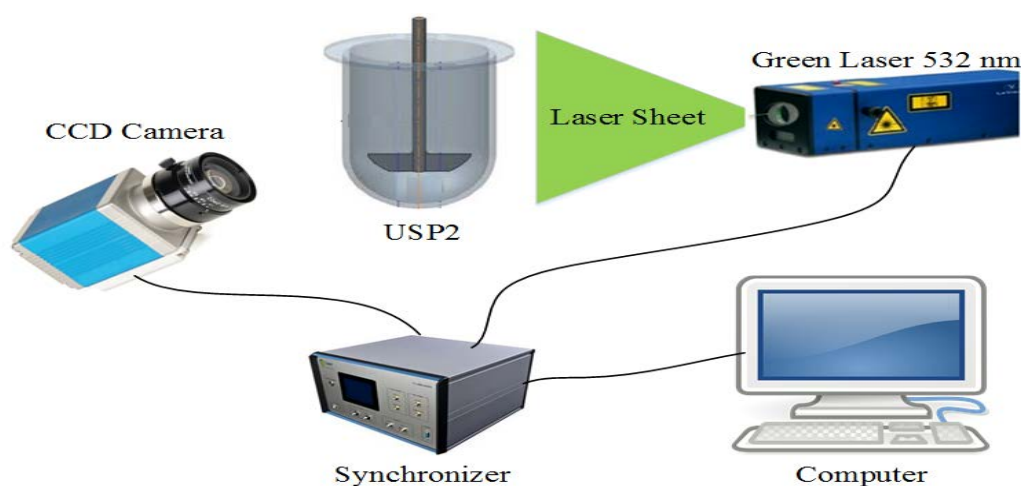


**Figure 2.** Schematic of an experimental setup for PIV tests.

## 2.3. Computational fluid dynamics (CFD)

Thanks to the recent advances in computer technology in computational fluid dynamics algorithms, CFD techniques are being

increasingly used as an effective tool to simulate and design the flow field in process equipment [24, 25]. The numerical simulation of the flow inside the 500-ml USP 2 vessel

was carried out at the two agitation rates used in the PIV experiments. Typically, such a simulation goes through four main steps:

1. Creating the geometry of the desired structure,
2. Meshing the created geometry,
3. Solving the energy, momentum, and mass balance equations for velocity and pressure fields at each node across the mesh for the time-dependent and time-independent cases.
4. Using solver results to analyze the hydrodynamics and fluid flow characteristics.

In this study, all of the mentioned steps were carried out by utilizing COMSOL Multiphysics 5.2 to determine the magnitude and direction of velocity and scalar value of local velocity at each point inside the vessel. As shown in Fig. 3, tetrahedral elements [26] were used to mesh the structure (normal mesh). To converge the responses, the mesh size was Minimized through several steps, and this process continued until the responses

were converged and the independency from the mesh was ensured. In order to evaluate the effects of changes in a real design on the resultant performance, the proposed simulated model could serve as a fast and cost-effective tool. In this research, the physics of the turbulent flow was selected to simulate the desired process. The mixed fluid was water, and the flow was assumed to be turbulent due to its higher value of paddle Reynolds number. Time-dependent fluid flow was solved within 21 s and 13.125 s at the agitation rates of 66 and 133 rpm, respectively, showing that 35 paddle revolutions are required to reach the operating conditions of the USP 2. The model was solved by means of two different methodologies. To this end, firstly, the model was solved using the Frozen Rotor method. The Frozen Rotor solution was, then, used as an initial condition for the time-dependent simulation.

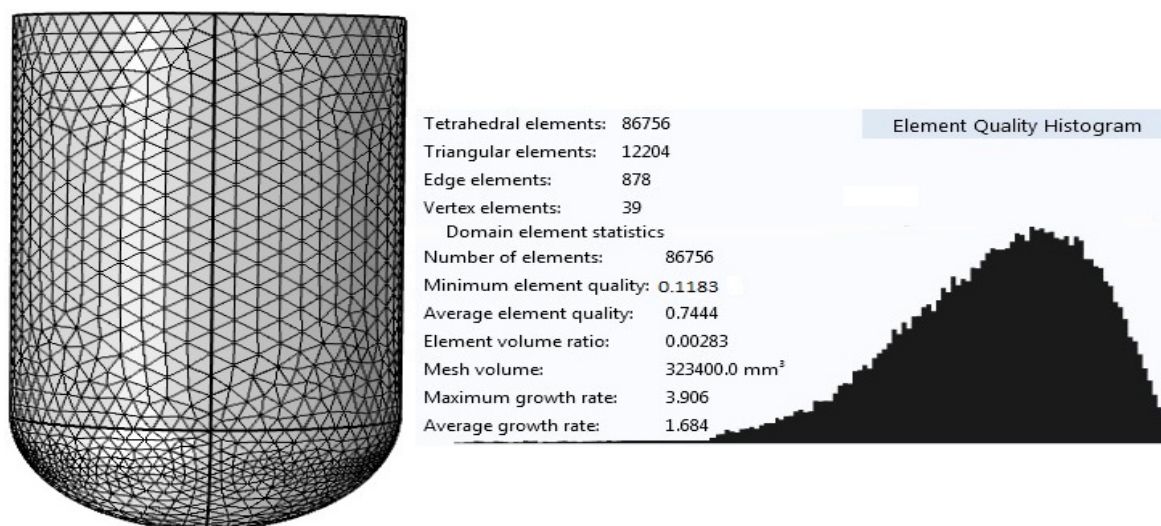


Figure 3. Surface mesh and mesh quality of small-volume USP 2 used for CFD calculation.

### 3. Results and discussion

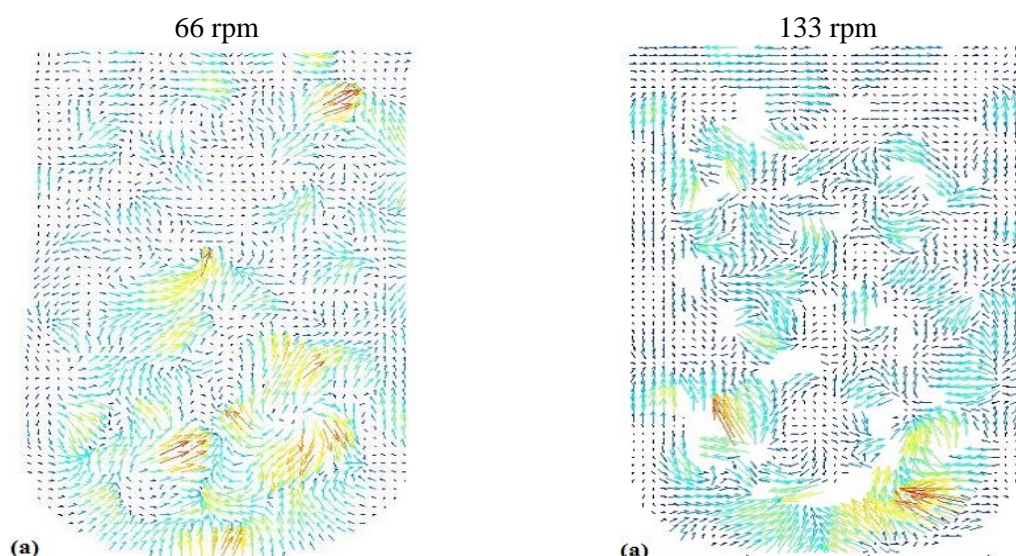
#### 3.1. Velocity field and magnitude

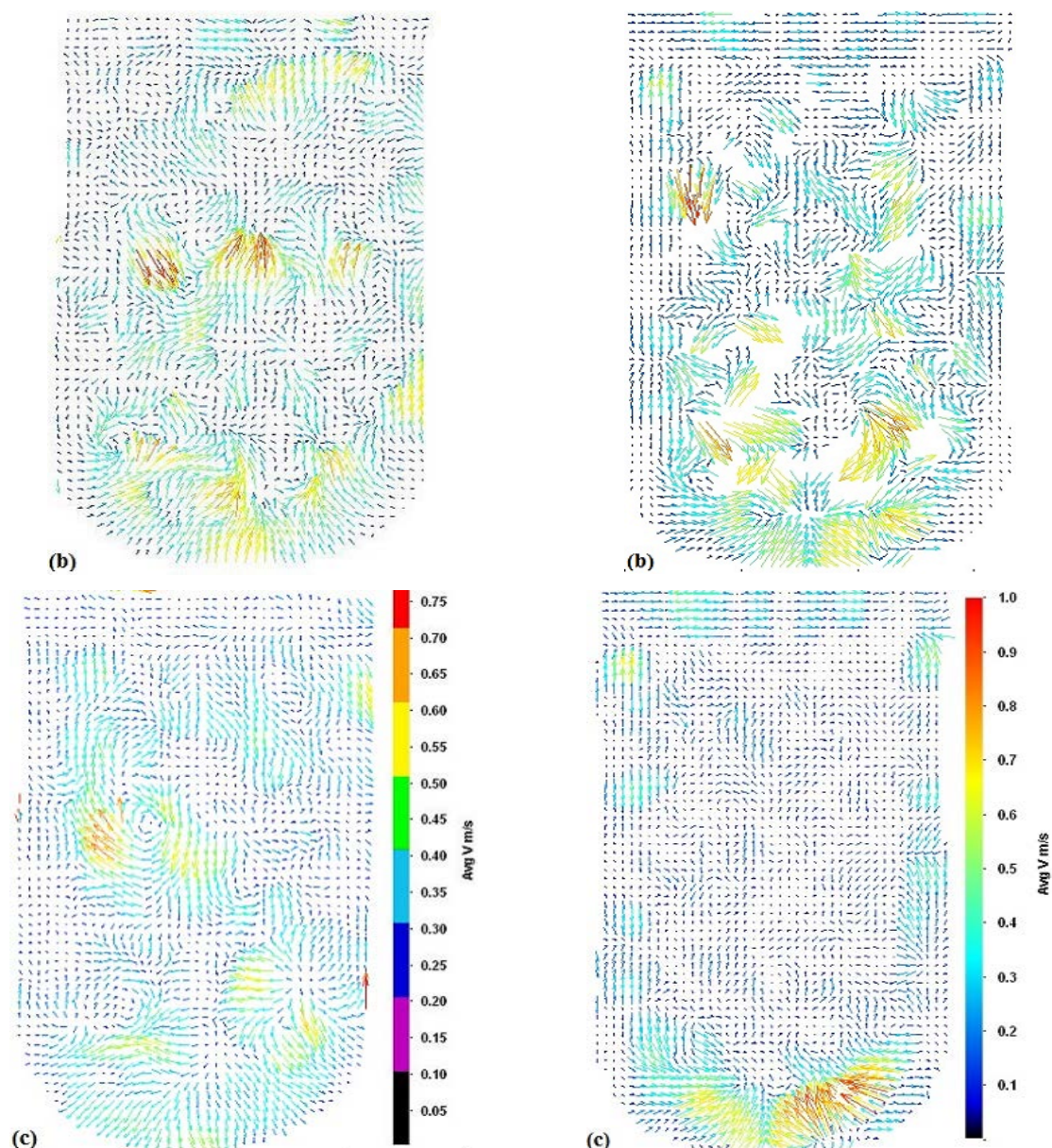
In mixing systems, the flow regime presents effective information about the pattern of

fluid flow. Similar to other agitation vessels, flow behavior in the USP-2 apparatus is characterized by Reynolds number  $Re = \frac{\rho ND^2}{\mu}$ , where  $\rho$  is the fluid density,  $N$  is the paddle

agitation rate,  $D$  is the paddle diameter, and  $\mu$  is the fluid viscosity. Accordingly, the flow regime will be either laminar, in transition state, or turbulent for  $Re < 10$ ,  $10 < Re < 1000$ , and  $Re > 1000$ , respectively. According to the agitation rates corresponding to 66 and 133 rpm, the flow regime in 500-ml USP 2 apparatus is turbulent. Fig. 4 shows instantaneous and time-averaged velocity field measurements by PIV experiments at Reynolds numbers of 2749 and 5541 on the plane of the paddle. The images represent the instantaneous velocity field in seconds, showing significantly different and asymmetric values unlike those of the velocity field calculated by the COMSOL Multiphysics Software. Generally, turbulent flows are time-dependent and experience a continuous reorientation of streamlines at specified times, especially at early times of the process. Therefore, the flow pattern might change at an early time of the process, ending up with a fully-developed turbulent flow. It is also worth noting that in some simulations and even laboratory experiments, despite its turbulent-oriented nature, the fluid flow pattern may relatively follow the same pattern from the beginning to the end of the process. This effect was observed in the flow pattern

obtained by means of COMSOL Multiphysics for the USP 2 utilized in this research. In order to measure the time-averaged velocity field, 300 images acquired in PIV experiments were averaged. Fig. 4 shows that the turbulent velocity field, where flow streamlines follow different directions, is time dependent. Therefore, instantaneous turbulent flows are unsteady; yet, sometimes, these flows are steady in terms of time-averaged velocity, despite differences in the amplitude of fluctuations and development of eddies in fully developed turbulent flow, which are favorable for micro-mixing but rather unfavorable for macro-mixing, consistency, and reproducibility of the system. During the dissolution and release tests, large eddies could move separated pieces of the tablet in the dissolution apparatus, leading to a heterogeneous and uncontrolled release of the drug. Fig. 4 shows that the paddle rotation tends to create an upward flow at the bottom of the vessel, where the tablet is placed. This flow could erode the tablet, pick up small pieces, and move them to the upper zones of the vessel. Even during tablet motion, it might collide with the paddle, leading to disintegration and, hence, more system variability.





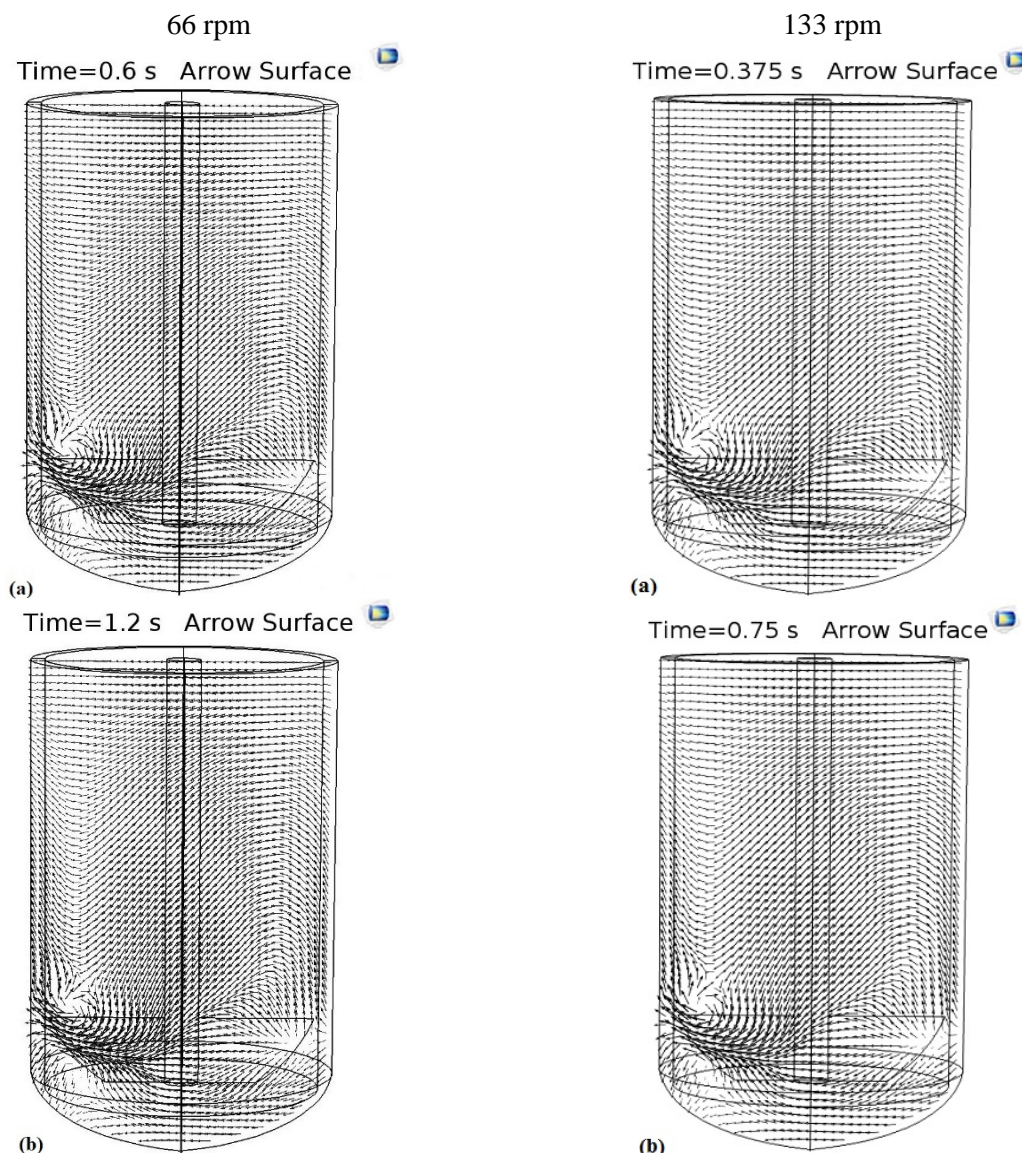
**Figure 4.** Instantaneous (a, b) and time average (c) velocity fields measured by PIV in the plane of the paddle.

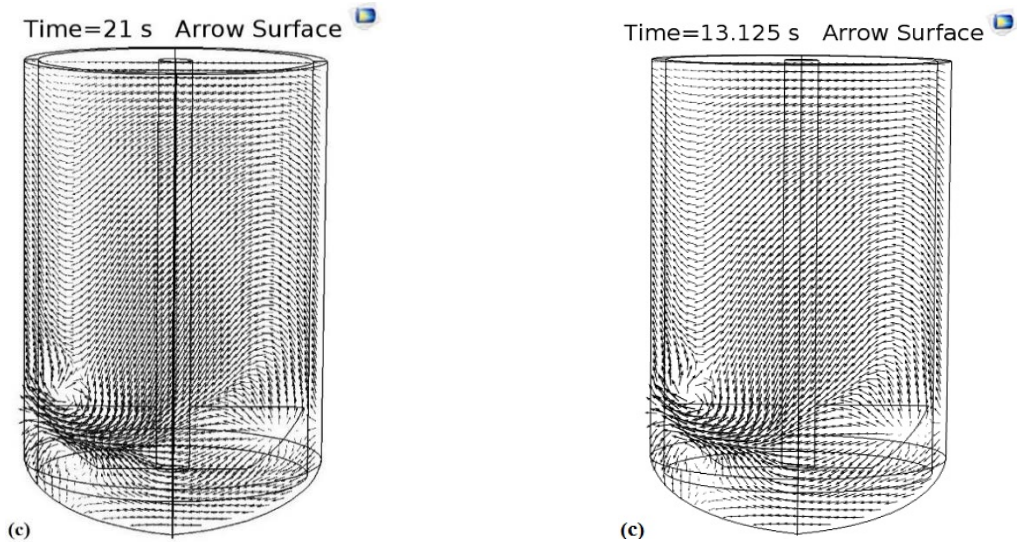
Fig. 5 shows the velocity field of the 500-ml USP 2 as calculated by COMSOL Multiphysics at two different paddle agitation rates on the plane of the paddle. The figure indicates similar flow behaviors at two Reynolds numbers corresponding to the agitation rates of 66 and 133 rpm. Therefore, an asymmetric pseudo-steady flow is likely to be observed from the CFD standpoint, not PIV on the plane of the paddle. Paddle rotation causes a divergent expansion flow at

the right edge of the paddle, thereby generating a rotational flow in the left half of the vessel. The divergent expansion flow is composed of two radial and axial components, with an upper part of the flow that generates a recirculation zone at the upper edge of the paddle as one moves leftward in the vessel, and a lower part of the flow that develops a recirculation zone at the lower edge of the paddle. In dissolution and release tests, the fluid rotation in recirculation

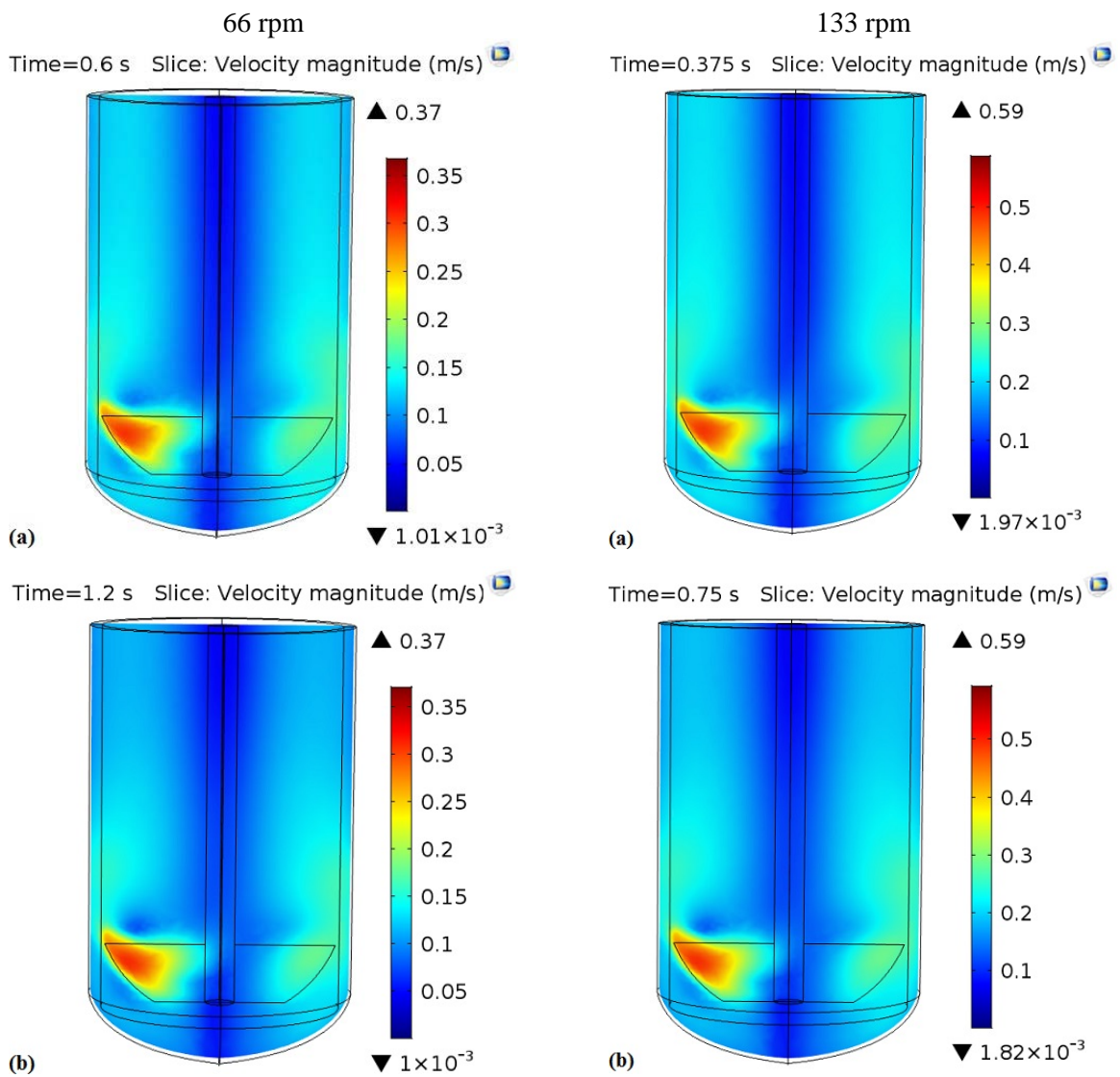
zones inhibits the entrance of API inside these zones by the paddle's convective mixing mechanism. Therefore, the paddle's upper and lower recirculation zones are representatives of the dead zones. At the bottom of the paddle, where the drug tablet is placed during the dissolution and release tests, the fluid flow is completely radial. Therefore, during the dissolution test, a shear force parallel to the upper surface of the tablet is applied to the tablet, leading to accelerated erosion. Fig. 6 shows the predicted magnitude of velocity on the plane of the paddle at two agitation rates of 66 and 133 rpm, as formerly calculated using COMSOL Multiphysics.

According to the figure, the distribution of velocity across the specified plane is asymmetric and the maximum velocity occurs at side edges of the paddle. Moreover, the minimum velocity occurs around the shaft and bottom of the vessel. Like the flow pattern characterized by velocity vectors, the distribution of velocity at different points in time (0.6 s corresponding to 1 revolution of the paddle, 0.375 and 1.2 s corresponding to 2 revolutions of the paddle, and 0.75, 21 and 13.125 s for 35 revolutions of the paddle) was approximately uniform, while the velocity magnitudes at agitation rates of 66 and 133 rpm were significantly different.





**Figure 5.** Instantaneous (a, b) and time-average fully-developed (c) velocity field simulations on the plane of the paddle after a) 1 revolution of the paddle, b) 2 revolutions of the paddle, and c) 35 revolutions of the paddle.



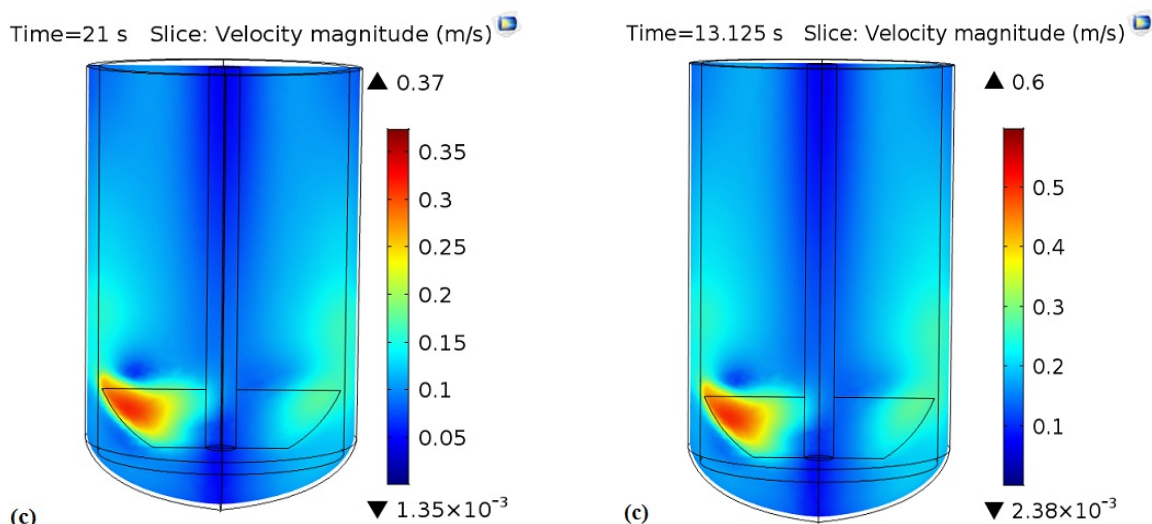
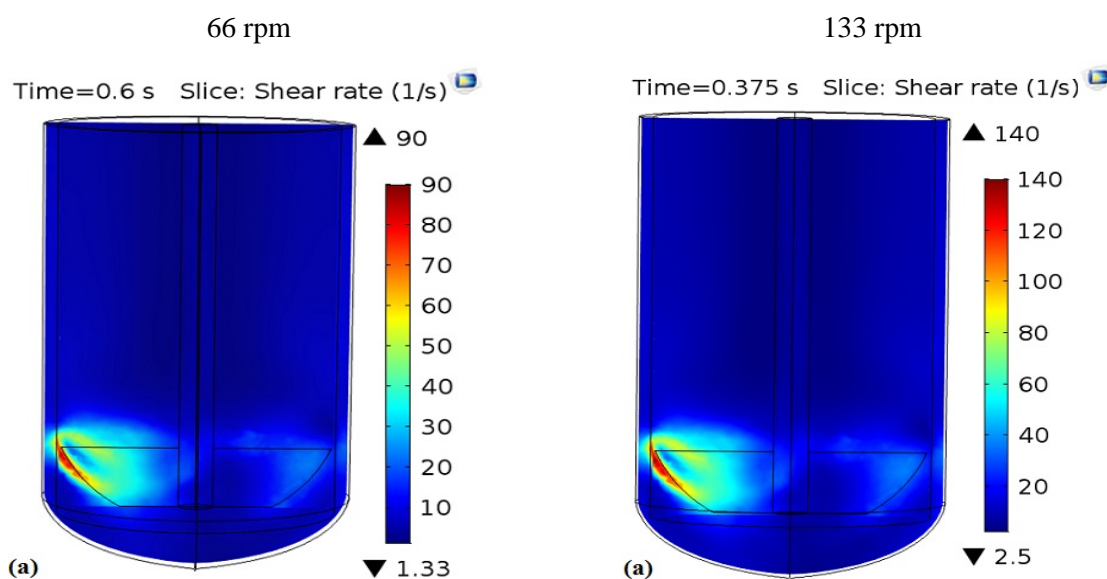


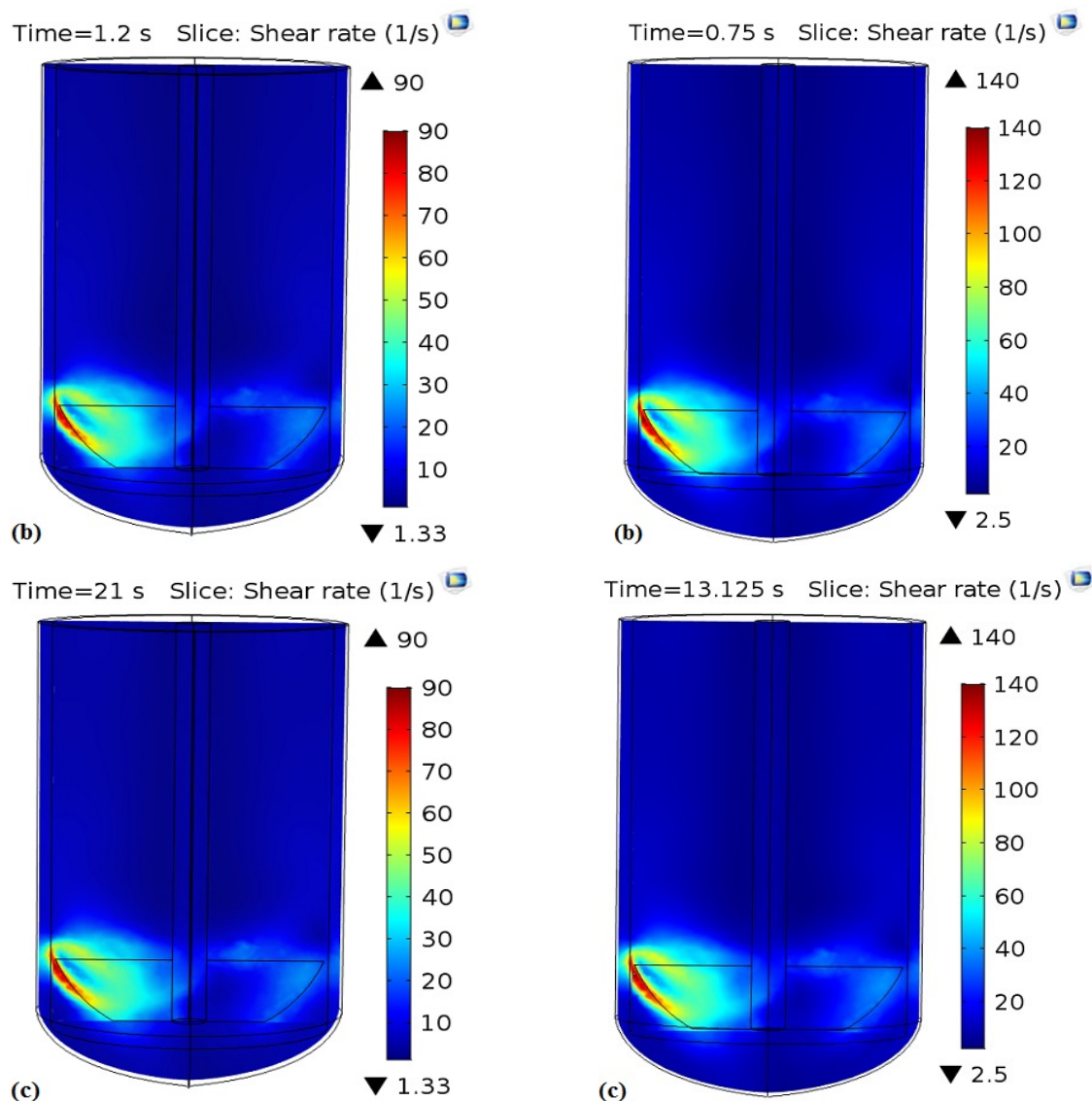
**Figure 6.** Instantaneous (a, b) and time-average fully-developed (c) velocity magnitude simulations on the plane of the paddle after a) 1 revolution of the paddle, b) 2 revolutions of the paddle, and c) 35 revolutions of the paddle.

### 3.2. Shear rate distribution

The study of shear forces in a dissolution test apparatus is of considerable importance because once swallowed, solid dosage forms enter a dynamic environment of the stomach where they are affected by physiological stresses and peristaltic waves of the stomach. These physiological stresses of the stomach along with muscle contractions cause mixing of the stomach contents and tablet disintegration that, ultimately, release API. Shear rate prediction by COMSOL

Multiphysics on the plane of the paddle is demonstrated in Fig. 7. The distribution of shear stress at different points in time at paddle speeds of 66 and 133 rpm follows the same patterns. It is observed that the shear rate increases by as much as 35 % by increasing the agitation rate from 66 rpm to 133 rpm, but its value remains approximately constant during the process. The maximum shear was observed around the paddle while its minimum value occurred around the shaft and bottom of the vessel.





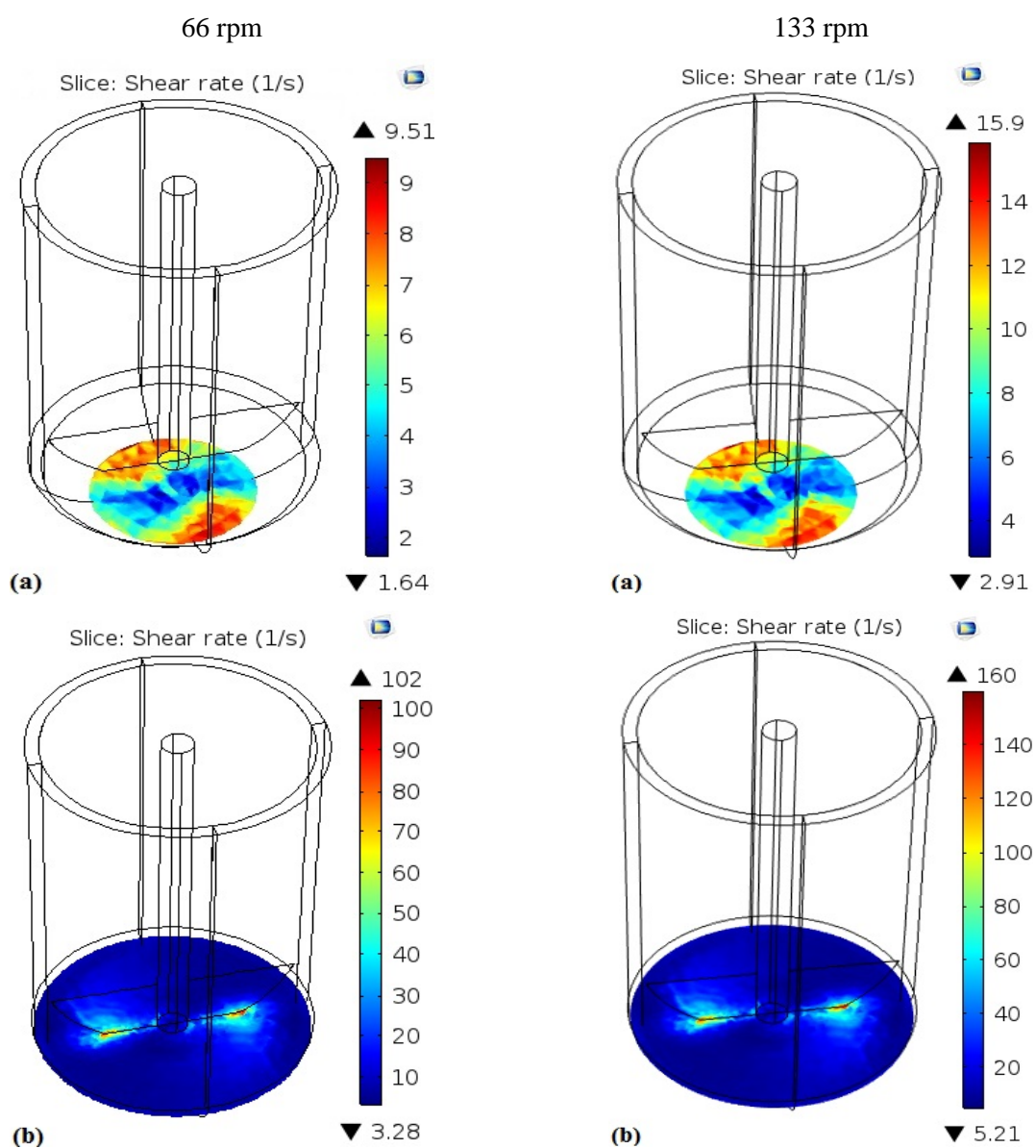
**Figure 7.** Shear rate simulations at feed state and fasted state on the plane of the paddle after a) 1 revolution of the paddle, b) 2 revolutions of the paddle, and c) 35 revolutions of the paddle.

Fig. 8. demonstrates the shear rate obtained by COMSOL Multiphysics across iso-surfaces parallel to the upper surface of the tablet. These shears are simulated for a better understanding of the effect of the shear stress the fluid has on the tablet. Fig. 8 clearly shows that the distribution of shear stress across the upper zone of the paddle follows a rotational pattern. At the center of this zone, shear forces are small, but they quickly increase as one gets farther from the center. By increasing the agitation rate, the applied shear stress from the fluid inside the vessel

increases as well. By affecting both transfer and dissolution of drug substance, the thickness of the boundary layer on the tablet surface is controlled by the fluid's shear forces. Distribution of shear stress across the plane at the bottom of the vessel plays an important role in disintegrating the matrix containing API and API release. As shown in Fig. 8., the distribution of shear stress across the plane at the bottom of the vessel (Fig. 8. a.) is asymmetric and its value increases as one moves from the plane center toward the vessel wall. Therefore, it can be stipulated

that during the dissolution test, the thickness of boundary layer at tablet edges is less than that at its center; therefore, the tablet starts to erode and disintegrate from the edges. On the planes parallel to the paddle's upper and lower surfaces (Figs. 8.b. and 8.c.), higher shear rates are observed along the plane centerline, with a maximum value reached at the paddle edge. This is due to the higher paddle tip rate. Across the mentioned iso-surfaces, the distribution of shear stress is asymmetric. In addition, the distribution of shear stress across the plane tangent to the

upper surface of the paddle and that at the bottom vessel where the tablet is placed during the dissolution test indicates the higher and lower values, respectively. It was found that the shear stress increased as one moved from the bottom of the vessel to the upper surface of the paddle, while the shear stress decreased as one moved from the upper surface of the paddle to the fluid surface. In order to demonstrate this fact, the shear rate data in the cutline along the vessel are plotted in Fig. 9 by COMSOL Multiphysics.



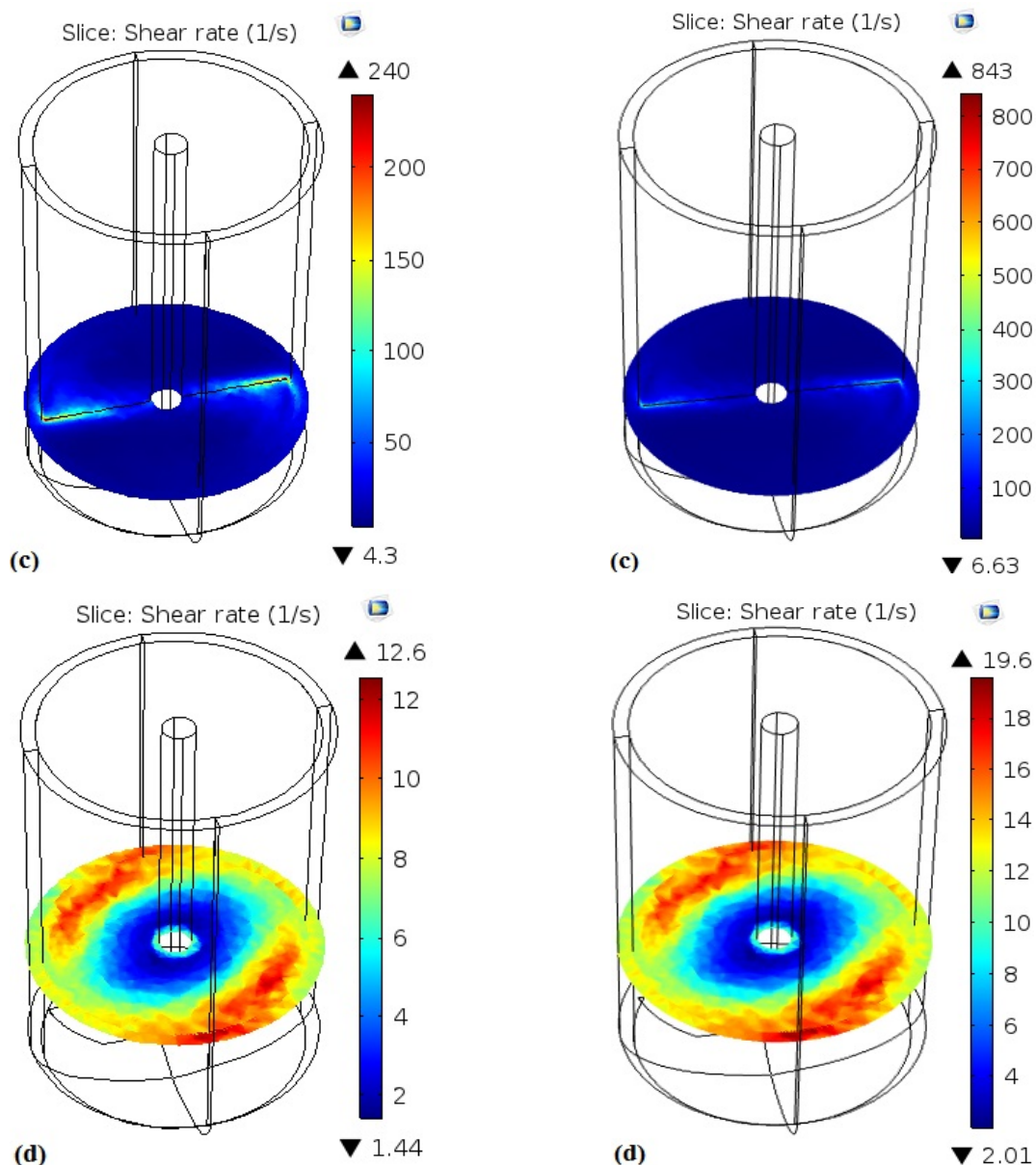


**Figure 8.** CFD simulations of shear rate on different iso-surfaces at a)  $y = -17$  mm, b)  $y = -4.3$  mm, c)  $y = 12.8$  mm and d)  $y = 30$  mm.

Fig. 9 illustrates that the shear rate increases while moving from the bottom of the vessel to the upper surface of the paddle and decreases while moving from the upper surface of the paddle to the free fluid surface. Of note, in this figure, the major hydrodynamic effects caused by paddle rotation are limited to the fluid around the paddle, while the other zones are affected by the shear stress applied by paddle rotation only partially. It is evident that, in the upper zones of the vessel, very

low velocity and uniform flow pattern are developed. API would be partially transferred to the upper zones of the vessel through a convective mechanism during tablet dissolution and release tests. Therefore, the concentration of the pharmaceutical ingredients released in these zones will be lower, and approximately constant, during the course of the test, making it impossible to collect samples from these zones to obtain the release profile.

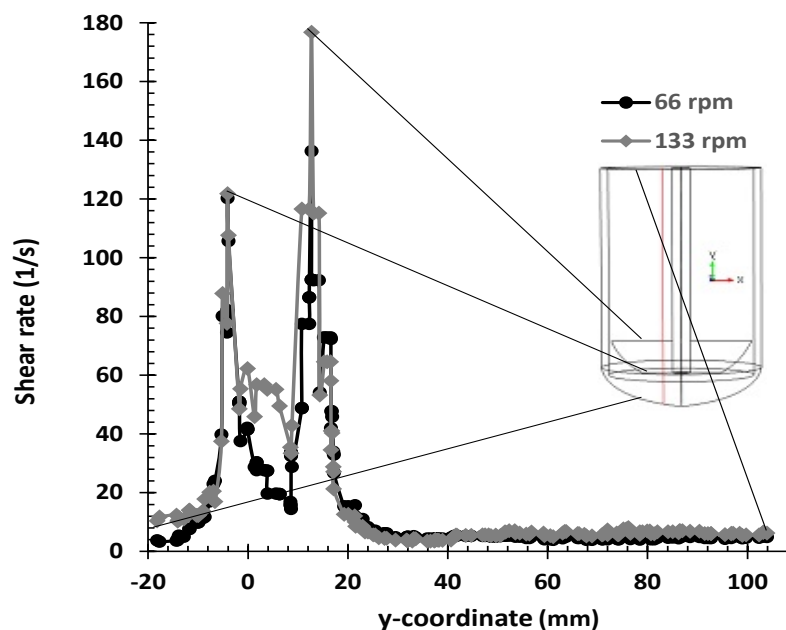


Figure 9. CFD simulation of shear rate in the cut line along the vessel.

### 3.3. Velocity profiles

Velocity magnitude profiles were obtained using PIV and COMSOL Multiphysics along four transverse cutlines along the vessel at paddle speeds of 66 and 133 rpm, corresponding to typical agitation speeds of standard USP 2 (Fig. 10 and 11). According to the figures, at the bottom of the vessel ( $y = -17$  mm), the velocity profiles obtained by PIV and CFD were significantly different despite the similar followed procedures. In experimental works, it has been shown that some of the parameters affecting the process are out of control and, rather, are randomly involved in the process as a result of natural causes, thereby imposing significant effects on the final result. Such parameters are as follows: personal errors, systematic errors, fluid temperature fluctuations inside the vessel, ambient air temperature fluctuations, etc. Basically, none of them in simulations has been taken into account. In the PIV technique, the hydrodynamic analysis of fluid flow is carried out by introducing specific particles into the fluid flow and considering

those moving in line with the flow inside the vessel. In simulations, however, no excipient other than the fluid itself was taken into consideration, and many assumptions and simplifications were made. Furthermore, as far as the evaluation of the velocity field is concerned, PIV is based on image processing, while CFD has its basis in solving energy, mass, and momentum balance equations for velocity and pressure fields simultaneously. Accordingly, experimental data and simulation results typically exhibit significant differences. Fig. 10. shows that the velocity results obtained by CFD and PIV along the cutlines  $y = -4.3$  mm (the one tangent to the lower surface of the paddle),  $y = 12.8$  mm (the one tangent to the upper surface of the paddle), and  $y = 30$  mm (the one parallel to the other cutlines at a height of 30 mm of the vessel) follow similar trends in the right half of the vessel. In the left half of the vessel, the difference between the experimental data and predicted results can be attributed to the difference between PIV and CFD techniques. In Fig. 11., changes in velocity along the four

cutlines followed the same pattern despite the difference between actual values of PIV- and CFD-obtained data. At both agitation speeds of the paddle, the highest velocities were observed along the cutline tangent to the upper surface of the paddle ( $y = 12.8$  mm) where the paddle rotation exerted maximum shear stress on the fluid around the paddle. However, minimum velocity along the specified cutline occurred at its middle point ( $x = 0$  mm). This point corresponds to the center of the bottom of the vessel, mid-point of the lower and upper diameters of the paddle, and center of the shaft for  $y = -17$  mm,  $y = -4.3$  mm,  $y = 12.8$  mm, and  $y = 30$

mm, respectively. From Figs. 10. and 11., it can be concluded that along the cutlines  $y = -17$  mm and  $y = 30$  mm, which correspond to the lower and upper parts of the paddle, respectively, the fluid close to the vessel wall shows maximum velocity. This happens as a result of pumping the fluid by the paddle toward the vessel wall and reinjecting the fluid from the wall into the paddle. This was further observed in the flow fields obtained by PIV and CFD techniques. The paddle tip ( $x = \pm 32$  mm and  $x \pm 18.15$  mm) exhibited maximum velocity along the cutlines tangent to the upper and lower surfaces of the paddle ( $y = 12.8$  mm and  $y = -4.3$  mm).

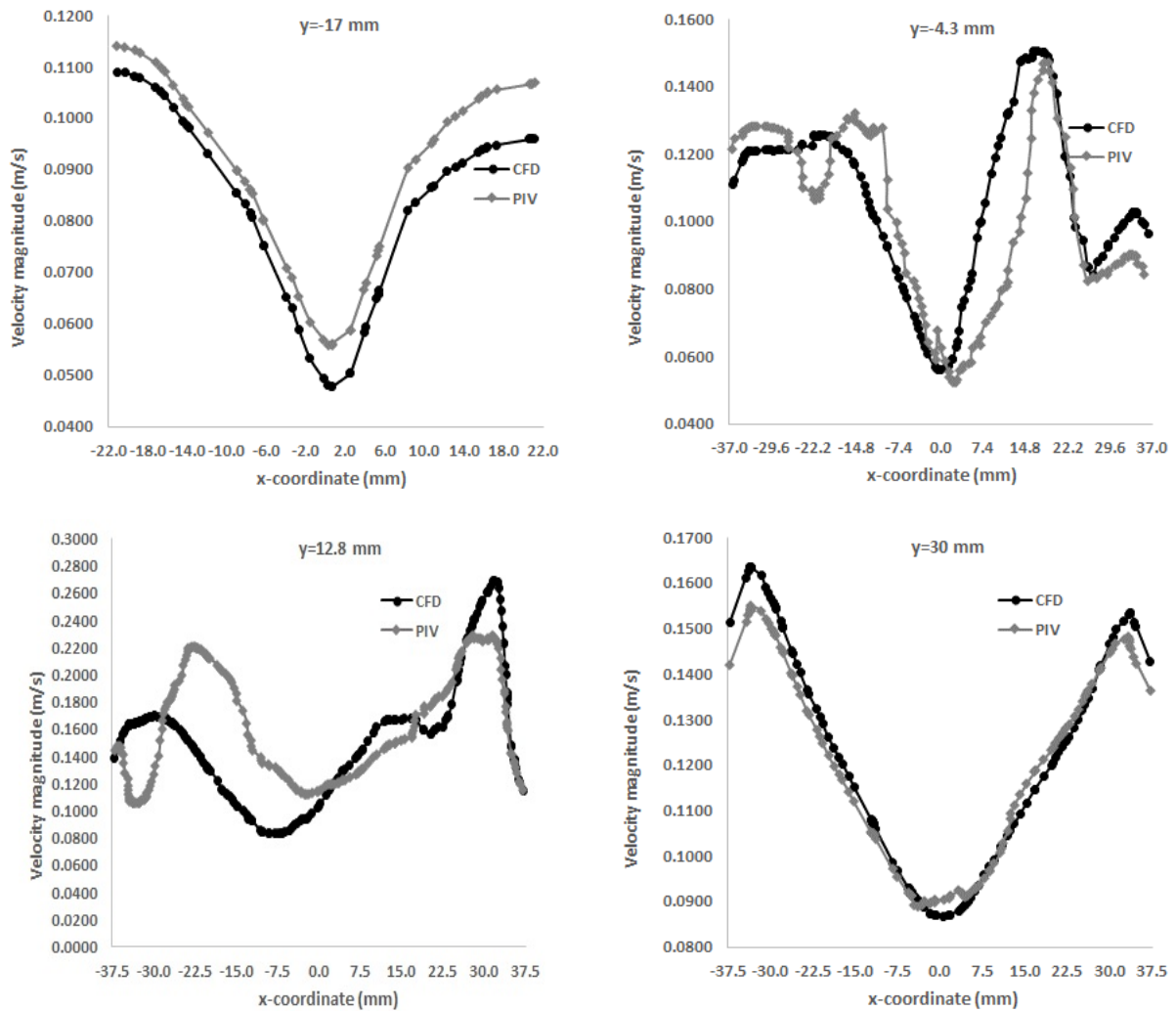


**Figure 10.** Comparison between experimental PIV velocity data and CFD predictions at an agitation speed of 66 rpm on different iso-surfaces.

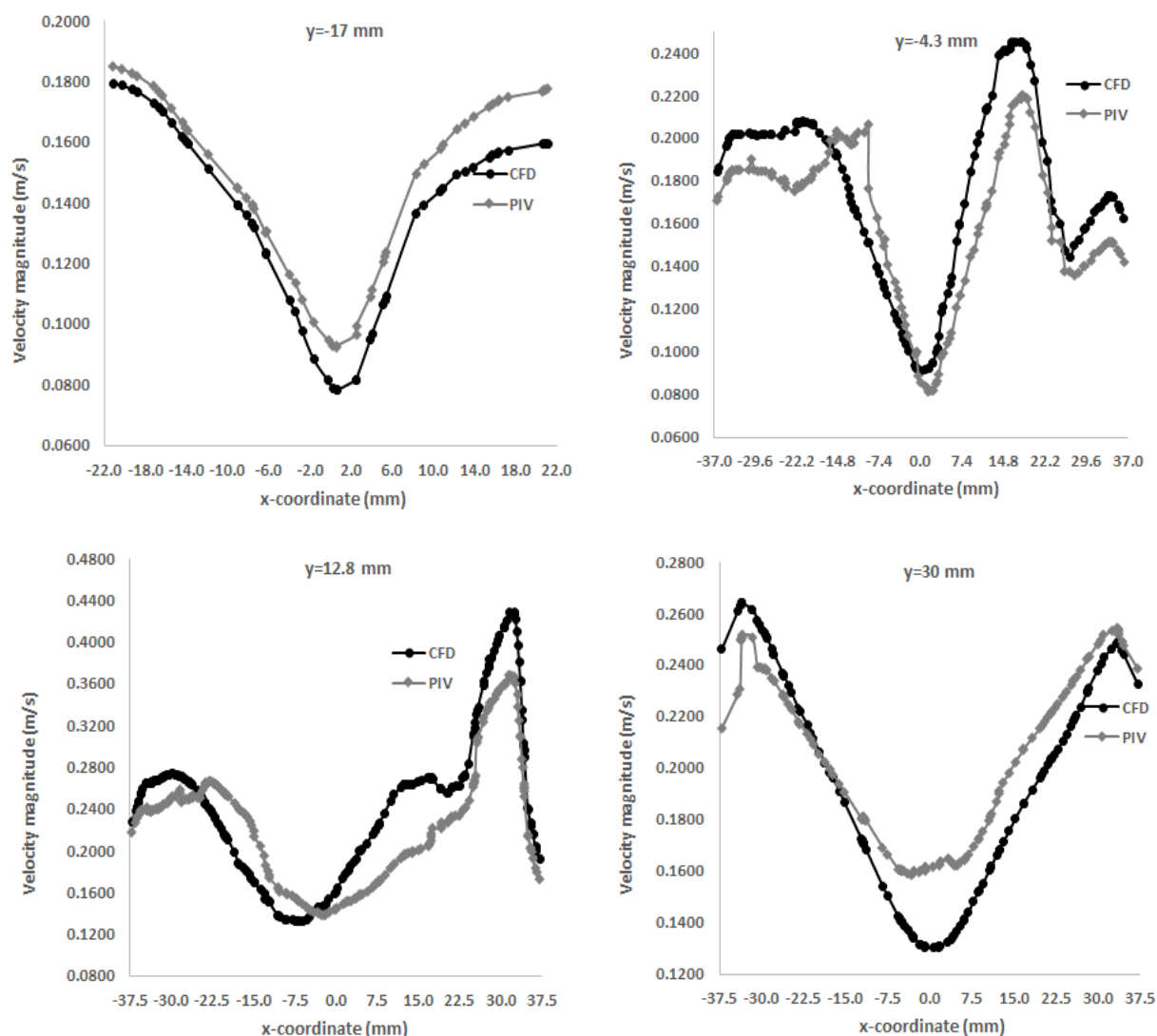


**Figure 11.** Comparison between experimental PIV velocity data and CFD predictions at an agitation speed of 133 on different iso-surfaces.

#### 4. Conclusions

In order to regulate the application of small-volume USP 2 apparatus, related standards and specifications should be incorporated into the United States Pharmacopeia. Therefore, in this study, a 500-ml USP 2 was designed and manufactured following the downscaling rules and the apparatus hydrodynamics was studied using two engineering tools, namely PIV and CFD, at two agitation rates of 66 and 133 rpm, corresponding to paddle agitation speeds of 50 and 100 rpm, respectively, in the standard USP 2 apparatus. Instantaneous and time-averaged velocity fields across the plane

tangent to the shaft were obtained by two simulators: PIV and COMSOL Multiphysics. The PIV results indicated that the velocity field was time-dependent and the orientation of streamlines and velocity vectors changed frequently. Investigations of the turbulent flow using PIV revealed the presence of fluctuations of various amplitudes and eddies. These secondary flows, desirable for micro-mixing, are recognized as undesirable for system consistency and reproducibility due to the unreliability and unpredictability of the samples taken from these zones. Unlike PIV results, the velocity field obtained by CFD did

not show much dependence on time, indicating a fully-developed fluid flow. The distribution of the predicted velocity across the plane tangent to the shaft was asymmetric, indicating the maximum velocity at the paddle tip. The distribution of the predicted shear stress across iso-surfaces cutting through the vessel showed that the shear increased from the bottom of the vessel to the upper surface of the paddle, but decreased from the upper surface of the paddle to free surface of the fluid. The comparison between velocity profiles along cutlines along the vessel showed that changes in experimental and predicted velocities followed approximately similar trends.

### Acknowledgement

This research did not receive any specific grant from funding agencies in the public, commercial, or not-for-profit sectors.

### Nomenclature

USP	United State pharmacopeia.
PIV	particle image velocimetry.
API	active pharmaceutical ingredient.
LDA	laser doppler anemometry.
CFD	computational fluid dynamic.
PLIF	planer laser-induced fluorescence.
LDV	laser doppler velocimetry.
CCD	charged-coupled device.
Rpm	round per minute.

### Symbols

$D_s$	diameter of standard vessel.
$V_s$	empty volume of the standard vessel.
$V_m$	empty volume of the model vessel.
$D_m$	diameter of model vessel.
$N_s$	agitation speed of the standard paddle.
$N_m$	agitation speed of the model paddle.
$(D_{pu})_m$	upper diameter of the model paddle.
$(D_{pl})_m$	lower diameter of the model paddle.
$H_{pm}$	height of the model paddle.
$C_m$	clearance between the bottom of the model paddle and the bottom of the model vessel.
$H_m$	height of the model vessel.
$H_s$	height of the standard vessel.

$D_{pu}$	upper diameter of standard paddle.
$D_{pl}$	lower diameter of standard paddle.
$H_p$	height of the standard paddle.
	clearance between the bottom of the standard paddle and the bottom of the standard vessel.
$C_s$	

### Greek letters

$\rho$	density [ $\text{gcm}^{-3}$ ].
$\mu$	viscosity [ $\text{gcm}^{-1}\text{s}^{-1}$ ].

### References

- [1] Wang, B. and Armenante, P. M., "Experimental and computational determination of the hydrodynamics of mini vessel dissolution testing systems", *International Journal of Pharmaceutics*, **510**, 336 (2016).
- [2] Kukura, J., Baxter, J. L. and Muzzio, F. J., "Shear distribution and variability in the USP Apparatus 2 under turbulent conditions", *International Journal of Pharmaceutics*, **279**, 9 (2004).
- [3] Gray, V., Kelly, G., Xia, M., Butler, C., Thomas, S. and Mayock, S., "The science of USP 1 and 2 dissolution: Present challenges and future relevance", *Pharmaceutical Research*, **26**, 1289 (2004).
- [4] Bai, G., Wang, Y. and Armenante, P. M., "Velocity profiles and shear strain rate variability in the USP dissolution testing apparatus 2 at different impeller agitation speeds", *International Journal of Pharmaceutics*, **403**,1 (2011).
- [5] Kong, F. and Singh, R. P., "Disintegration of solid foods in human stomach", *Journal of Food Science*, **73**, 67 (2008).
- [6] Stamatopoulos, K., Batchelor, H. K., Alberini, F., Ramsay, J. and Simmons, M. J. H., "Understanding the impact of media viscosity on dissolution of a highly water soluble drug within a USP 2 mini vessel dissolution apparatus using

- an optical planar induced fluorescence (PLIF) method”, *International Journal of Pharmaceutics*, **495**, 362 (2015).
- [7] Kukura, J., Arratia, P. E., Szalai, E. S. and Muzzio, F. J., “Engineering tools for understanding the hydrodynamics of dissolution tests”, *Drug Development and Industrial Pharmacy*, **29**, 231 (2004).
- [8] Maderuelo, C., Zarzuelo, A. and Lanao, J. M., “Critical factors in the release of drugs from sustained release hydrophilic matrices”, *Journal of Controlled Release*, **154**, 2 (2011).
- [9] Bahari, N., Omid, N. J., Moosavi, N., Shirmard, L. R., Tehrani, M. R. and Dorkoosh, F., “Preparation, statistical optimization and in vitro evaluation of pramipexole prolonged delivery system based on poly (3-hydroxybutyrate-co-3-hydroxyvalerate) nanoparticles”, *Journal of Drug Delivery Science and Technology*, **44**, 82 (2018).
- [10] Xu, W., Gao, Q., Xu, Y., Wu, D., Sun, Y., Shen, W. and Deng, F., “Controllable release of ibuprofen from size-adjustable and surface hydrophobic mesoporous silica spheres”, *Powder Technology*, **191**, 13 (2009).
- [11] Klein, S., “The mini paddle apparatus—A useful tool in the early developmental stage? Experiences with immediate-release dosage forms”, *Dissolution Technology*, **13**, 6 (2006).
- [12] Emmanuel, S., Marc, L., Eric, B. and Michel, C. J., “Small volume dissolution testing as a powerful method during pharmaceutical development” *Pharmaceutics*, **2**, 351 (2012).
- [13] Stamatopoulos, K., Alberini, F., Batchelor, H. and Simmons, M. J. H., “Use of PLIF to assess the mixing performance of small volume USP 2 apparatus in shear thinning media”, *Chemical Engineering Science*, **145**, 1 (2016).
- [14] Aoki, S., Ando, H., Ishii, M., Ida, K., Watanabe, S. and Ozawa, H., “Evaluation of the correlation between in vivo and in vitro release: Effect of the food of contraction and food on drug release”, *Biological and Pharmaceutical Bulletin*, **17**, 291 (1994).
- [15] United States Pharmacopeia and National Formulary, The United States Pharmacopeial Convention, Stage 6 Harmonization Official, (December 1, 2011).
- [16] Bocanegra, L. M., Morris, G. J. and Jurewicz, J. T., “Fluid and particle laser doppler velocity measurements and mass transfer predictions for the USP paddle method dissolution apparatus”, *Drug Development and Industrial Pharmacy*, **16**, 1441 (1990).
- [17] Baxter, J. L., Kukura, J. and Muzzio, F. J., “Hydrodynamics-induced variability in the USP apparatus II dissolution test”, *International Journal of Pharmaceutics*, **292**, 17 (2005).
- [18] Bai, G., Armenante, P. M., Plank, R. V., Gentzler, M., Ford, K. and Harmon, P., “Hydrodynamic investigation of USP dissolution test apparatus II”, *Journal of Pharmaceutical Sciences*, **96**, 2327 (2007).
- [19] Siewert, M., “FIP guidelines for dissolution testing of solid oral products (final draft, 1995)”, *Drug Information Journal*, **30**, 1071 (1996).
- [20] Luyben, A. M., Heijnen, J. J., VanderLans, R. M. and Potters, J. J. M., “Lecture notes on scale-up/scale down”, Delft University of Technology, Faculty

- of Applied Sciences, Department of Biotechnology, (2006).
- [21] Prasad, A. K., Adrian, R. J., Landreth, C. C. and Offutt, P. W., “Effect of resolution on the speed and accuracy of particle image velocimetry interrogation”, *Experiments in Fluids*, **13**, 105 (1992).
- [22] Hartl, K. A. and Smits, A. J., “PIV measurements in fire whirls”, *Experiments in Fluids*, **60**, 1 (2019).
- [23] Zhang, L., Li, Z., Yang, N., Jiang, B., Cong, H. and Zhang, Z., “Hydrodynamics and mass transfer performance of vapor–liquid flow of orthogonal wave tray column”, *Journal of the Taiwan Institute of Chemical Engineers*, **63**, 6 (2016).
- [24] Zadghaffari, R., Moghaddas, J. S. and Revestedt, J., “A study on liquid-liquid mixing in a stirred tank with a 6-blade rushton turbine”, *Iranian Journal of Chemical Engineering (IJChE)*, **5** (4), 12 (2008).
- [25] Vakili, M. H. and Nasr Esfahani, M., “CFD investigation of hydrodynamics in an industrial suspension polymerization mixing reactor”, *Iranian Journal of Chemical Engineering (IJChE)*, **9** (2), 43 (2012).